Pergamon

J. Mech. Phys. Solids, Vol. 42, No. 7, pp. 1139–1158, 1994
Copyright © 1994 Elsevier Science Ltd
Printed in Great Britain. All rights reserved
0022 5096/94 $7.00+0.00

0022–5096(94)E0022–V

ON LARGE SCALE SLIDING IN FIBER-REINFORCED COMPOSITES

Z. CEDRIC XIA, JOHN W. HUTCHINSON, ANTHONY G. EVANS† and BERNARD BUDIANSKY

Division of Applied Sciences, Harvard University, Cambridge, MA 02138, U.S.A.; and † Materials Department, University of California, Santa Barbara, CA 93106, U.S.A.

(*Received* 9 *December* 1993)

ABSTRACT

A CRITICAL EXAMINATION is made of the use of the line spring model to represent fiber bridging of matrix cracks in the analysis of failure phenomena in fiber-reinforced brittle matrix composites. Attention is focused on composite systems designed to undergo fiber debonding and sliding when matrix cracking occurs. For most composites of this class, it is found that the distance along the fiber within which sliding occurs is often too large to justify use of the line spring representation. A model which allows for large scale sliding (the LSS model) is proposed and applied to three problems: a matrix crack emerging from a semi-infinite unbridged through-crack in a uni-directional fiber-reinforced composite, the same problem for the finite length unbridged through-crack, and matrix cracking of a cross-ply composite. Primary emphasis is placed on the stress concentration in the bridging fibers. Predictions from the LSS model are compared with those from the line spring model. In general, the line–spring model is found to overestimate the stress concentration in critically located fibers. A discussion of the significance of the lower estimates of the stress concentration factors is given for several composite systems.

NOMENCLATURE

c_f, c_m	fiber, matrix volume fractions ($c_f + c_m = 1$)
E	longitudinal Young's modulus, $= c_f E_f + c_m E_m$
E_f, E_m	fiber, matrix Young's moduli
l	length of the sliding zone
R_f	fiber radius
σ_f	tensile stress in the bridging fibers
$p = c_f \sigma_f$	smeared-out bridging stress in the bridging fibers
τ	interface sliding shear stress

1. INTRODUCTION

HIGH STRENGTH CERAMIC fibers are employed to enhance the fracture performance of ceramic matrices. A well designed composite can sustain matrix cracks traversing the composite. Unbroken, debonded fibers then provide bridging restraint across the matrix crack faces. After the matrix is fully cracked, the intact fibers continue to carry additional load. Eventually the fibers fail and the composite ruptures, but the load-bearing capacity may substantially exceed the stress for matrix cracking.

An approach to studying matrix cracking and fiber stress concentrations in fiber-reinforced composites has emerged, wherein a line–spring model is used to represent the effect of intact fibers bridging matrix cracks. If the radius and spacing of the fibers are small compared to other length scales characterizing the deformation of the composite, the bridging-fiber forces can be smeared-out and treated as stresses provided by springs connecting crack faces. A bridging law is then used to relate the spring stress to the crack opening displacement. If the fiber–matrix interface has negligible debonding energy, if initial stresses are ignored, and if a constant frictional sliding stress τ is assumed, the following nonlinear bridging law results from an elementary shear lag analysis:

$$p(x) = \beta\sqrt{\delta(x)/2}, \tag{1}$$

where $p(x)$ is the smeared-out fiber bridging stress and $\delta(x)$ is the effective opening displacement along the bridged region. The nonlinear spring constant β is given by

$$\beta = \left\{\frac{4c_f^2 E_f E^2 \tau}{R_f c_m^2 E_m^2}\right\}^{1/2}, \tag{2}$$

where the notation is defined in the Nomenclature. The distance along the fiber l, within which sliding occurs on each side of the crack surface, is related to the smeared-out fiber bridging stress by

$$l(x) = \frac{c_m E_m R_f}{2c_f E\tau} p(x). \tag{3}$$

The bridging law is consistent with l greater than several fiber radii.†

The bridging law can be used together with integral equation methods to formulate and solve various problems for stresses in bridging fibers and stress intensity factors of matrix cracks. Thus, for example, it was in this way that MARSHALL *et al.* (1985) and MCCARTNEY (1987) obtained conditions for the spread of a matrix crack from an initial, finite length bridged matrix crack. The critical stress required to propagate the matrix crack approaches the steady-state cracking stress for a semi-infinite bridged matrix crack, originally obtained by energy-based analyses by AVESTON *et al.* (1971) and BUDIANSKY *et al.* (1986). MARSHALL and COX (1987) and BUDIANSKY and CUI (1994) have used the line–spring approach based on (1) to study the effect of an unbridged through-crack in a uni-directional composite on the subsequent propagation of a matrix crack extending from the through-crack. These authors also determine the maximum stress experienced by the bridging fibers as the matrix crack spreads. Given the strength of the fibers, they estimate the ultimate strength of the composite as a function of initial through-crack flaw size. With much the same aim,

† Readers should be aware that the bridging law (1, 2) is not exactly the same as some in the earliest papers on the subject. The formula for β by MARSHALL *et al.* (1985) and MARSHAL and COX (1987) is missing a factor $[c_m E_m/E]^{1/2}$. MARSHALL and COX (1988) give a formula identical to that given here. MCCARTNEY's (1987) formula is also the same as the present one, apart from a factor $1-\nu^2$. The transverse interaction between the fiber and the matrix due to Poisson contraction can be approximated in various ways leading to such minor variations in the law [see discussion in the Appendix of HE *et al.* (1993)]. More recently, MEDA and STEIF (1993) proposed a modification of the bridging law with a nonzero bridging stress as δ becomes zero.

XIA and HUTCHINSON (1994) have used the line–spring approach to investigate matrix cracking and fiber stress concentration in cross-ply composites.

Line–spring models have become valuable tools in the micromechanics analysis of various toughening mechanisms [see BAO and SUO (1992) for a review]. These models replace bridging elements by an equivalent traction–displacement law applied as a boundary condition along the crack line. For the fiber bridging model, the constituent properties of the composite and the interface are nicely incorporated into one single spring parameter, β. In addition, the spring model allows use of well established analytical techniques to solve crack bridging problems. As convenient and powerful as the line–spring model appears to be, suspicions have arisen that results obtained from this model for fiber stress concentration in the presence of through-cracks may be unduly high. Specific experimental evidence giving rise to these suspicions is cited in Section 6 of this paper, where it is noted that the ultimate strength of some cross-ply composites should not be as high as experimentally measured, given the stress concentration levels predicted in the fibers by the line–spring model. It was this apparent discrepancy between theory and experiment which motivated a critical examination of the line–spring model for this application, and which led to the identification of large scale sliding (LSS) as one possible source of the discrepancy.

The large scale sliding model is proposed in the next section, and a solution procedure using this model is outlined. It is then applied to three representative problems in subsequent sections: (i) the asymptotic problem for a semi-infinite through-crack collinear with a semi-infinite bridged matrix crack (Fig. 1); (ii) a finite length through-crack with fully extended collinear matrix cracks [see ahead to Fig. 5(a)]; and (iii) a multiply cracked cross-ply laminate [see ahead to Fig. 5(b)]. For each problem, key parameters of the problem are identified and solutions based on the line–spring model are obtained. The new LSS model is then applied to the problem, and the results are compared with those from the line–spring model. For composite constituent properties chosen within practical ranges, substantial reductions of stress concentration in the most highly stressed fibers just ahead of the through-crack tip are predicted by the LSS model relative to the line–spring model. At the same time, it is demonstrated that line–spring results are applicable when the constituent properties are such that small scale sliding does occur. Summary discussion is given in the last section, along with the appraisal of the experimental observations alluded to above.

2. THE LARGE SCALE SLIDING MODEL

The uni-directional fiber-reinforced composite containing a semi-infinite through-crack with a fully extended matrix crack will be used to introduce the LSS model. As shown in Fig. 1, the crack is loaded by a remote, mode I field specified by the monotonically increasing stress intensity factor K_I. Plane strain conditions are assumed for the composite blocks, and the mode I field is that for a crack in an elastically orthotropic solid. The primary quantity of interest is the stress in the leading fibers just ahead of the through-crack tip, at $x = 0$.

The line–spring model is indicated in the lower left-hand corner of Fig. 1. The

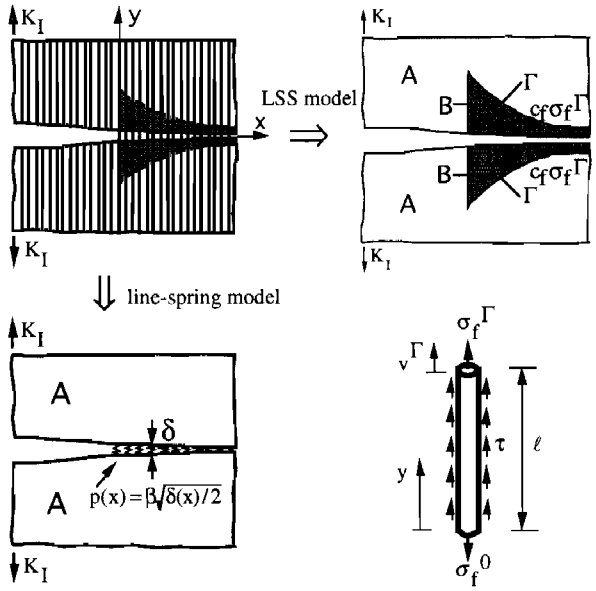

FIG. 1. A semi-infinite, unbridged through-crack with a semi-infinite, collinear bridged matrix crack. Conventions for the line–spring model and the large scale sliding model.

traction–separation law (1) and (2) is applied as a boundary condition along the x-axis, for $x > 0$. In region A, outside the sliding zone, the solid is characterized by the orthotropic elastic behavior of the composite, i.e. the matrix material reinforced by perfectly bonded, uni-directional fibers. A nonlinear integral equation for the distribution of the opening displacement $\delta(x)$ is formulated. Solution of this equation provides both the opening displacement and the distribution of the stress in the fibers where they cross the x-axis, ahead of the through-crack tip. Details of this solution will be given in the next section.

The rationale for a line–spring approximation requires that the extent of sliding be small compared to all relevant in-plane lengths. Only then can a sliding zone of finite width be confidently replaced by an equivalent traction–displacement condition applied along a line. In the present problem of Fig. 1, there is only a single characteristic length parameter, described in the next section. In the other problems, additional relevant lengths may be pertinent, such as the length of a through-crack or, in the case of the cross-ply composite, the ply thickness.

The LSS model distinguishes between region B in which fiber sliding has occurred and region A in which it has not. Within B, the fibers are treated separately from the matrix, as will be made clear in the sequel. Denote the boundary between regions A and B by Γ, characterized by the extent of fiber sliding $l(x)$. This boundary is not known in advance but must be determined as part of the solution process. If it is assumed that sliding is one-signed, consistent with K_I being monotonically increased, the load transfer from the fibers to the matrix, within B, is known precisely. Because each sliding fiber exerts a force per unit length on the matrix equal to $2\pi R_f \tau$, the load transfer from fibers to matrix within B is equivalent to a body force per unit volume given by

$$f = \frac{2c_f\tau}{R_f}. \tag{4}$$

It acts in the sense shown in Fig. 1, required by symmetry with respect to the x-axis. Denote the stress in a fiber at the line of the matrix crack on $y = 0$ by σ_f^0, and denote its value at the top of the slipped region at $y = l$ by σ_f^Γ. A simple shear lag analysis based on equilibrium of the fiber (see Fig. 1) and compatibility of strain at the top of the sliding zone requires

$$\sigma_f^\Gamma = \sigma_f^0 - \frac{2\tau}{R_f} l, \tag{5a}$$

$$\frac{\sigma_f^\Gamma}{E_f} = \frac{c_f\sigma_f^0}{E}. \tag{5b}$$

These combine to give

$$l = \frac{c_m E_m R_f}{2E\tau}\sigma_f^0. \tag{6}$$

In addition to the body force f in region B, the sliding fibers exert a line load (load per unit thickness per unit length in the x-direction) along Γ equal to $c_f\sigma_f^\Gamma$. The one remaining quantity needed to fully describe the behavior of the slipping segment of a fiber is its vertical displacement v^Γ at the top of the slipped region. It is related to the other quantities by

$$v^\Gamma = \frac{1}{E_f}\left(\sigma_f^0 l - \frac{\tau}{R_f} l^2\right) \tag{7}$$

where, by symmetry, the vertical displacement of the fibers is zero along $y = 0$ for $x > 0$.

The LSS model is posed as follows. Assuming that the location of Γ is known (it must be determined by iteration), the sliding fibers may be regarded as separate entities from the rest of the solid in B. Represent the fibers as just described. Represent the remnant material in region B by a linear elastic material whose properties are those of the matrix with cylindrical holes rather than fibers. These are constrained only in the transverse direction, because the fiber and matrix remain in frictionless contact. This replacement will be specified more precisely below. The material in A is assigned the orthotropic moduli of the composite with bonded fibers. The loads on the planar body comprising the composite in region A and the remnant matrix in region B are the remote K_I-field, the vertical body force f in B, and the vertical line load $c_f\sigma_f^\Gamma$ acting along Γ. The remnant matrix in B has zero tractions acting along the matrix crack line ($y = 0$, $x > 0$). The separate sliding fibers in B are governed by the *three* equations (5a), (6) and (7) and are described by *four* unknowns, σ_f^Γ, σ_f^0, l and v^Γ. The deformation of the sliding segments of the fibers is coupled to the planar body specified above by requiring that v^Γ coincide with the vertical displacement of the body on Γ, i.e. $v^\Gamma(x) = v(x, l(x))$.

In a given iteration with $l(x)$ regarded as known, the system of equations for the

body in regions A and B, together with (5a) and (7) for the sliding fiber segments and the coupling condition on Γ, specifies a solution for all field quantities, including the stresses in the fibers. In general, however, this solution will not be consistent with (6) specifying the vertical extent of the zone of sliding. Given σ_f^0 from the current iteration, (6) can be used to generate $l(x)$ for the next iteration. However performed, an *iteration process must be used to determine the location of* Γ.

Like the composite material in region A, the remnant matrix material in region B is orthotropic with one axis of orthotropy aligned with the y-axis. Transverse isotropy with respect to the y-axis would be assumed for both materials in most instances, and this has been done here. The moduli of the remnant material in B are those of the matrix material alone, but containing cylindrical holes with freely sliding fibers. Since the composites being considered in this paper are assumed to have a residual compression acting across the fiber–matrix interface, the sliding fibers in region B continue to constrain the behavior of the remnant matrix by frictionless contact. Various methods are available for estimating the moduli of the remnant material. The one employed for the present problems will be mentioned in the next section. For the problems investigated in this paper, the main quantities of interest are rather insensitive to details of the elastic properties of the remnant matrix in B. In fact, it was found that the moduli of the material in A could be substituted for those for the remnant matrix in B with little consequence. The significance of this substitution is that the problem for the planar body in the combined regions A and B becomes elastically homogeneous, opening up such LSS problems to solution by analytical methods which could not otherwise be used.

In this paper the LSS problems have been analysed by accounting for the different elastic properties in regions A and B. A finite element method has been used for this purpose. Most aspects of the implementation of the model in a finite element code are standard. A finite element mesh is formed for the planar body in regions A and B. It is convenient to regard the separate sliding fibers in region B as a separate "fiber sheet" which has a Young's modulus $c_f E_f$ in the y-direction and all other moduli (including shear moduli) taken to be zero. The sliding stress τ acts on the fiber sheet as the body force f but in the direction opposite to that on the remnant matrix. The fiber sheet has zero vertical displacement along the x-axis and is attached to the planar body along Γ. This representation is readily implemented in the ABAQUS code used to carry out the computations. The fiber sheet representation is completely equivalent to (5a) and (7). As already mentioned, (6) is used to update the location of Γ for the next iteration when σ_f^0 has been determined.

3. A Matrix Crack Emerging from a Semi-infinite Through-crack

The problem addressed in this section is an asymptotic problem in which a matrix crack has extended from the tip of a semi-infinite through-crack which is loaded by a remote mode I field with stress intensity K_I. Two sub-problems are considered: the problem mentioned in connection with Fig. 1 where the bridged matrix crack extends to infinity, and a version of the same problem where the matrix crack has finite length a_m. The emphasis in the first problem will be on determination of the stress distribution

in the fibers where they bridge the matrix crack. The bridging stress of the leading fibers will also be of concern in the second problem, along with the stress intensity factor at the tip of the matrix crack. These quantities will be computed using both the line–spring model and the LSS model. The problem of Fig. 1 for the fully extended matrix crack is considered first.

A closed form expression can be readily obtained for the bridging stress of the leading fibers, $p_0 \equiv p(0) = p(\delta(0))$, as predicted by the line–spring model based on the bridging law (1). The following result is restricted to the problem at hand involving the fully expended matrix crack. Application of the J-integral to connect the remote field to the opening along the crack faces gives

$$J = \frac{K_I^2}{A\bar{E}} = \int_0^{\delta(0)} p(\delta)\,\mathrm{d}\delta. \tag{8}$$

Here $\bar{E} = E/(1-\nu^2)$, where E is the Young's modulus of the composite for stressing parallel to the fibers, ν is the Poisson strain ratio of transverse contraction to axial elongation, and A is an orthotropy factor. This factor depends on c_f and on non-dimensional moduli combinations specifying the properties of the uni-directionally reinforced composite [see, for example, BUDIANSKY and CUI (1994)]. It is unity for an isotropic material and lies between 0.8 and 1 for most composites. Substitution of the bridging law (1) into (8) yields

$$p_0 = \left(\frac{3\beta^2 K_I^2}{4A\bar{E}}\right)^{1/3}. \tag{9}$$

Determination of the distribution of the bridging stress, $p(x)$, for the line–spring model requires the formulation and solution of an integral equation. These procedures are now well established; therefore, the equation and the numerical analysis used in its solution will not be recorded here. The analysis employed has been used by XIA and HUTCHINSON (1994) to study similar equations. The integral equation for $p(x)$ can be put in non-dimensional form using two quantities: the bridging stress at the tip, p_0, and a quantity with the dimensions of length,

$$d = \left(\frac{3A\bar{E}K_I}{\beta^2}\right)^{2/3}. \tag{10}$$

This is the only length parameter in the problem. Numerical results for the bridging stress $p(x)$ normalized by p_0 are plotted as a function of x/d in Fig. 2 as a solid line; note that the bridging stress p is $c_f\sigma_f$. The curve in Fig. 2 is universal in the sense that there is no additional parametric dependence. Included in Fig. 2 is the classical inverse square root stress distribution, $K_I/(2\pi x)^{1/2}$, specifying the remote field, which takes the form $p/p_0 = (2/3)^{2/3}/\sqrt{2\pi(x/d)}$. Note that the length quantity d characterizes the transition to the classical field, with any significant difference from it disappearing for x greater than about $1.5d$. The length of the sliding zone at the tip will be compared to d in the assessment of whether LSS conditions pertain.

Now consider the large scale sliding model of this problem. It is convenient to use

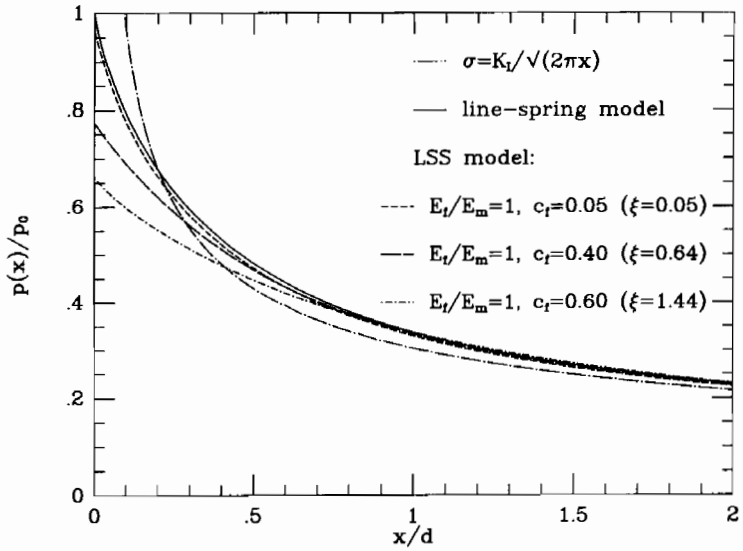

FIG. 2. Bridging stress distributions ahead of the through-crack tip.

the two quantities p_0 and d defined above. The formula (6) relating the slip length to the stress in the fibers along the line of the matrix crack ($y = 0$) can be rewritten as

$$\frac{l(x)}{d} = \left(\frac{2}{3}\right)^{1/3} \frac{c_f E_f E}{c_m E_m A \bar{E}} \frac{p(x)}{p_0}, \tag{11}$$

where now $p(x) = c_f \sigma_f^0(x)$. The body force f is given by

$$f = \frac{p_0}{d}\left(\frac{3}{2}\right)^{1/3} \frac{c_m^2 E_m^2 A \bar{E}}{c_f E_f E^2} \tag{12}$$

and the remotely applied stress intensity factor is linked to p_0 and d by

$$K_I = \left(\frac{2}{3}\right)^{2/3} p_0 \sqrt{d}. \tag{13}$$

It follows from (11)–(13) that, according to the LSS model, the stress distribution in the bridging fibers, normalized by p_0, will depend only on x/d, in addition to the non-dimensional moduli parameters characterizing the composite, such as E_f/E_m, and the fiber volume fraction c_f. In all the numerical examples presented in this paper the Poisson's ratios of the fiber and the matrix are taken to be the same and equal to 0.2. In the four problems studied in this paper, we have used HILL's (1965) self-consistent results for the transversely isotropic elastic properties of the composite in region A. The moduli in region B have also been represented as transversely isotropic and have been determined using the same self-consistent equations, but replacing fibers by cylindrical holes for the purpose of estimating the axial modulus, the Poisson's ratio relating the transverse and axial strains, and the longitudinal shear modulus. The transverse modulus and Poisson's ratio relating the two transverse strains were taken

to be the same as those of the composite with bonded fibers. This approximately accounts for the constraint afforded by contact across the fiber–matrix interface. The transversely isotropic properties were used to generate the plane strain moduli quantities needed in each of the problems studied here. The LSS model is now fully specified.

Numerical calculations were carried out for a wide range of E_f/E_m and c_f (with $\nu_f = \nu_m = 0.2$). To appreciate the numerical results, consider the ratio of the extent of sliding of the fibers at the through-crack tip to d as predicted by the line–spring model, i.e. with $p(0) = p_0$,

$$\frac{l(0)}{d} = \left(\frac{2}{3}\right)^{1/3} \frac{c_f E_f E}{c_m E_m \bar{A} \bar{E}} \equiv \left(\frac{2}{3}\right)^{1/3} \xi. \tag{14}$$

For typical values of the parameters appearing on the right-hand side of (14) the ratio of sliding length to d will not be small compared to unity. Only materials with small ξ will give rise to small values of this ratio. It will be seen that if ξ is not small the LSS predictions will differ appreciably from those of the line–spring model. This is illustrated by the LSS stress distributions for $E_f/E_m = 1$ and various c_f, covering a range of ξ, in Fig. 2. The LSS distributions progressively approach the distribution of the line–spring model for decreasing ξ. Of the examples shown, agreement arises only for $\xi = 0.05$ corresponding to the unrealistically small fiber volume fraction $c_f = 0.05$. Figure 3(a) presents LSS results for the stress in the fibers just ahead of the through-crack tip. The results are presented as the ratio $(c_f\sigma_f)_{LSS}/(c_f\sigma_f)_{lsm}$, where $(c_f\sigma_f)_{lsm} = p_0$ is the line–spring model prediction. This ratio reflects the extent to which the LSS prediction is lower than the line–spring prediction for the most severely stressed fibers. For all practical values of E_f/E_m and c_f, the line–spring model overestimates the fiber stress concentration substantially. Figure 3(b) reveals a remarkable near-collapse to a single relationship of all the numerical results in Fig. 3(a) when they are plotted as $(c_f\sigma_f)_{LSS}/(c_f\sigma_f)_{lsm}$ versus ξ. The solid line in Fig. 3(b) is an empirical curve fit to the numerical data. For this problem, Fig. 3(b) clearly shows that the parameter ξ provides a measure of the degree to which LSS predictions differ from the line–spring predictions. In turn, by (14), this confirms that the necessity of invoking an LSS approach is tied to the magnitude of the ratio of the sliding length at the through-crack tip to d.

A selected set of the above numerical computations with the LSS model were repeated with only a change in the elastic moduli in region B. We found very little sensitivity in the predictions for the fiber stresses to the details of the moduli in B. An excellent approximation to the results presented above was obtained by taking the moduli in B to be the same as those in A. Evidently, the essential difference between the LSS and line–spring models lies in the modeling of the spatial aspects of the load transfer from the fibers and not in complications of the modified moduli in region B. The finite height of the sliding zone at the tip of the through-crack tends to diffuse the stress concentration in the most highly stressed fibers.

Next consider a matrix crack of finite length a_m ahead the through-crack tip as shown in the insert in Fig. 4. Now the emphasis will be on the stress intensity factor K_t at the matrix crack tip, as well as the stress concentration in the fiber at the through-

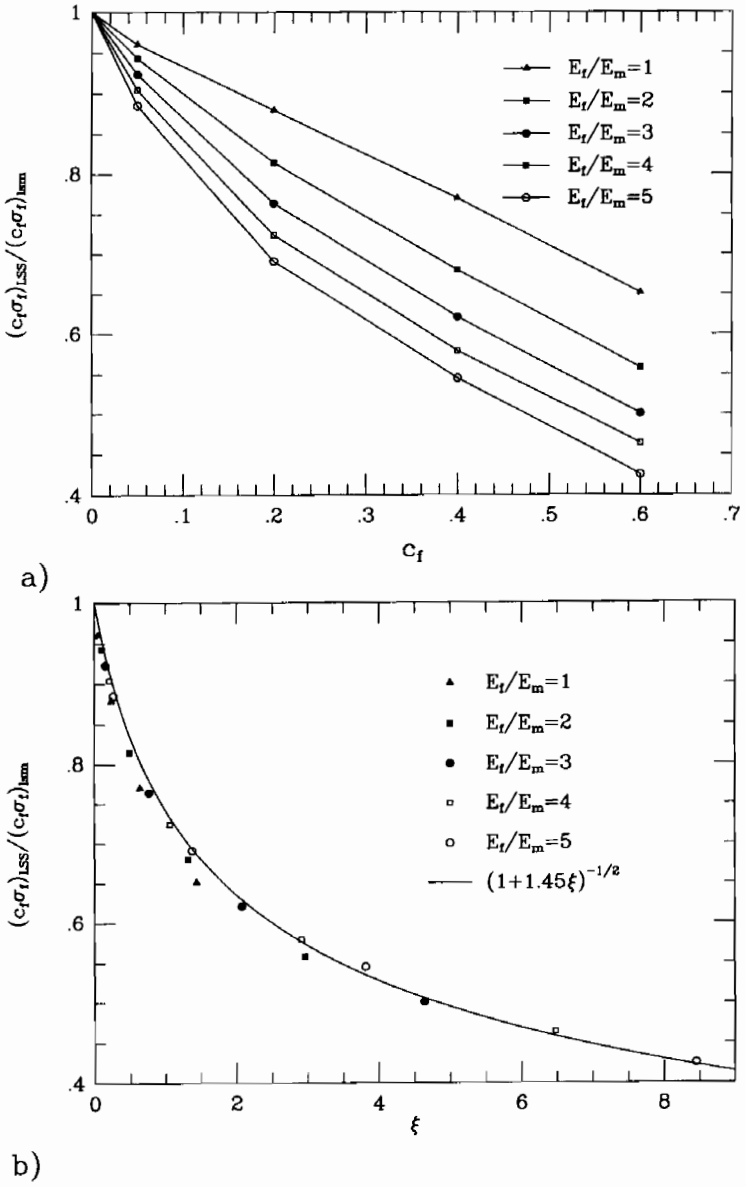

FIG. 3. (a) Ratio of the bridging stress directly ahead of the through-crack tip as predicted by the LSS model to that by the line–spring model [i.e. p_0 given in (9)]. (b) The ratio in (a) plotted against ξ defined in (14). The solid line curve is an empirical fit to the computed values.

crack tip. The line–spring model version of this problem was first solved for all values of a_m/d, and the results are presented in Fig. 4. Figure 4(a) displays K_t/K_I as a function of normalized matrix crack length, a_m/d, while Fig. 4(b) displays the companion plot of $c_f\sigma_f/p_0$ for the fibers just ahead of the through-crack tip. The portion of the curve for $a_m/d < 0.2$ has been dashed because the line–spring relation (1) is increasingly inaccurate as δ goes to zero, with the consequence that the prediction for the stress in

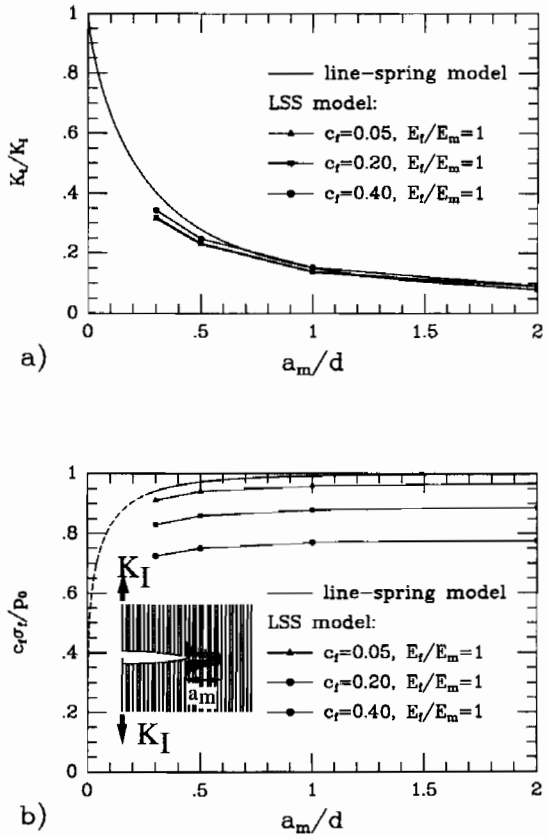

FIG. 4. (a) Ratio of the stress intensity factor of the bridged matrix crack to remote stress intensity factor as a function of the normalized matrix crack length. (b) Ratio of the bridging stresses just ahead of the unbridged through-crack as a function of the normalized matrix crack length as predicted by the two models.

the lead fiber is not expected to be correct when $a_m = 0$ (MEDA and STEIF, 1993). Also shown in Fig. 4 are numerical results obtained from the LSS model for $E_f/E_m = 1$ and several values of c_f, again chosen to illustrate the approach to the line–spring predictions when c_f (and thus ξ) becomes small. Differences between the predictions of the two models for the matrix crack stress intensity factor are relatively small. The substantial reductions in stress concentration in the lead fibers predicted by the LSS model compared to the line–spring model are seen to be only weakly dependent on a_m/d.

4. UNI-DIRECTIONAL COMPOSITE CONTAINING A FINITE THROUGH-CRACK AND FULLY EXTENDED MATRIX CRACKS

The second problem to be investigated using the LSS model is that of a uni-directional fiber-reinforced composite containing a finite through-crack of length $2a$

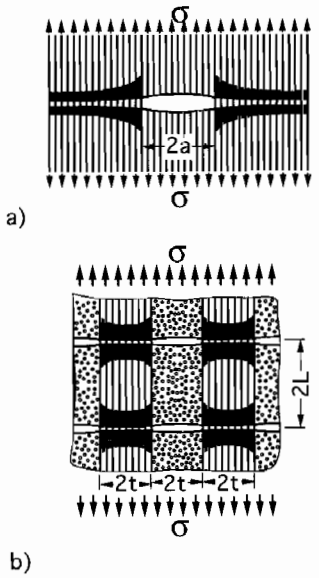

FIG. 5. Conventions. (a) Finite length unbridged through-crack with collinear semi-infinite bridged matrix cracks. (b) Transverse section of a cross-ply matrix with a uniform distribution of unbridged through-cracks in the 90° plies and bridged matrix cracks in the 0° plies.

with fully extended matrix cracks emerging from each tip, as depicted in Fig. 5(a). A remote stress σ acts on the composite. This problem was previously studied by BUDIANSKY and CUI (1994) by means of the line–spring model in an effort to determine the tensile strength of the composite in the presence of crack-like flaws. Determination of the stress concentration in the leading fiber ahead of the through-crack tip has special interest, because failure of the leading fibers will precipitate failure of the composite.

Define the stress concentration factor (SCF) for the leading fibers at the through-crack tip as

$$\lambda = \frac{c_f \sigma_f}{\sigma}, \tag{15}$$

where $c_f\sigma_f$ is again the smeared-out bridging stress of the leading fibers. Since the through-crack is not bridged by fibers, λ will exceed unity. The line–spring version of the problem is again obtained by formulating and solving an integral equation. In accordance with the analysis of Budiansky and Cui, the solution for λ is fully characterized by a single non-dimensional parameter, η, defined as

$$\eta = \frac{3\pi c_f^2 E_f E^2}{c_m^2 E_m^2 A\bar{E}} \frac{a\tau}{R_f \sigma}. \tag{16}$$

The relation between λ and η obtained from the numerical solution of the integral equation is plotted in Fig. 6(a) as the solid line. A remarkably accurate approximation to this result is given by

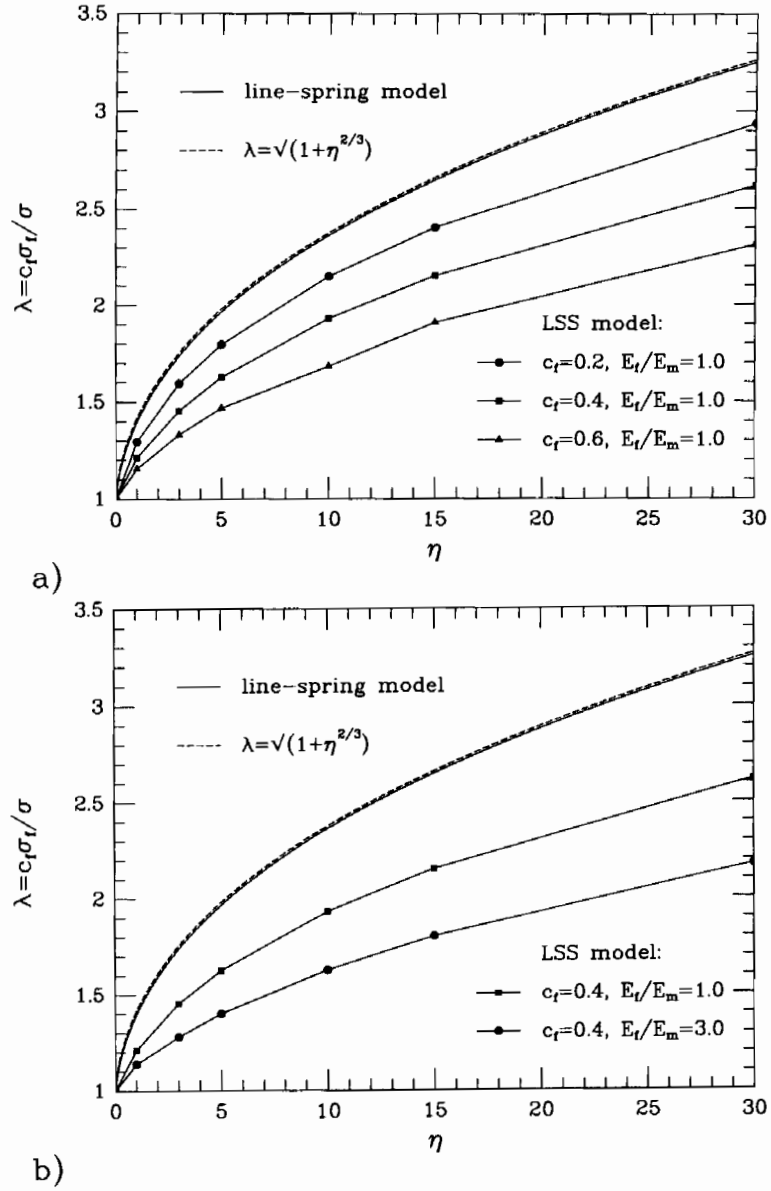

FIG. 6. Stress concentration factor for the bridging stress just ahead of a finite length through-crack as a function of η defined in (16) as predicted by the two models. (a) The effect of varying fiber volume fraction in the LSS model. (b) The effect of varying E_f/E_m in the LSS model.

$$\lambda = \sqrt{1+\eta^{2/3}} \tag{17}$$

shown as the dashed curve in Fig. 6(a) [obtained from (12) of Budiansky and Cui].

The LSS model is similar to that developed for the previous problem. The slip length in (3) is now normalized by the half-length of the unbridged through-crack and written as

$$\frac{l(x)}{a} = \frac{3\pi c_f E_f E}{2c_m E_m A\bar{E}} \frac{1}{\eta} \frac{p(x)}{\sigma} \tag{18}$$

and the body force f is expressed as

$$f = \frac{\sigma}{a} \frac{2c_m^2 E_m^2 A\bar{E}}{3\pi c_f E_f E^2} \eta. \tag{19}$$

It can now be shown from a non-dimensionalization of the governing equations for the LSS model that the SCF, λ, depends on η and on the non-dimensional parameters such as E_f/E_m and c_f specifying the composite.

There are two length quantities in this problem: the half-crack length a and the measure d which may still be defined as in (10), but now with $K_I = \sigma\sqrt{\pi a}$. To place the need for an LSS approach into perspective, the height of the sliding zone at the tip of the through-crack, $l(a)$, as predicted by the line–spring model will be compared to both a and d. By (15), the approximation (17), and (18),

$$\frac{l(a)}{a} = \frac{c_f E_f E}{c_m E_m A\bar{E}} \frac{3\pi\sqrt{1+\eta^{2/3}}}{2\eta} = \xi \frac{3\pi\sqrt{1+\eta^{2/3}}}{2\eta}. \tag{20}$$

A plot of $l(a)/(\xi a)$ versus η is given in Fig. 7(a). Similarly, the line–spring estimate of the other length ratio is

$$\frac{l(a)}{d} = \frac{c_f E_f E}{c_m E_m A\bar{E}} \frac{\sqrt{1+\eta^{2/3}}}{(3\eta/2)^{1/3}} = \xi \frac{\sqrt{1+\eta^{2/3}}}{(3\eta/2)^{1/3}} \tag{21}$$

and $l(a)/(\xi d)$ is also plotted in Fig. 7(a). For a given value of the parameter ξ, the ratio $l(a)/d$ is nearly constant over most of the range of η, while $l(a)/a$ is largest for small η and falls off gradually for large η. Based on experience with the previous problem, LSS conditions are again expected to depend on the magnitude of ξ as well as η.

Results obtained from the LSS model for three values of c_f with $E_f/E_m = 1$ ($\nu_f = \nu_m = 0.2$) are included in Fig. 6(a). The appreciable deviation between the two models with increasing c_f is clearly evident. The influence of a change in E_f/E_m is displayed in Fig. 6(b). It is apparent that the discrepancy between the two models is considerable over essentially the entire practical range of parameter space, with the LSS model predicting lower values of stress concentration. The numerical data points from the two plots of Fig. 6 for $\eta = 1$, 5 and 30 are used to plot the ratio $(c_f\sigma_f)_{LSS}/(c_f\sigma_f)_{lsm}$ as a function of ξ in Fig. 7(b). The lowest curve in this figure is the empirical fit to the numerical results for the semi-infinite through-crack problem in Fig. 3(b), which corresponds to the limit $\eta = \infty$. It can be noted that for η ranging from about 5 to ∞ the reduction in the LSS prediction for the stress in the leading fibers relative to the line–spring model depends primarily on ξ.

5. A Multiply Cracked Cross-ply Laminate

The last of the problems to be studied is a fiber-reinforced cross-ply laminate with unbridged through-cracks across the 90° plies connected by bridged matrix cracks in

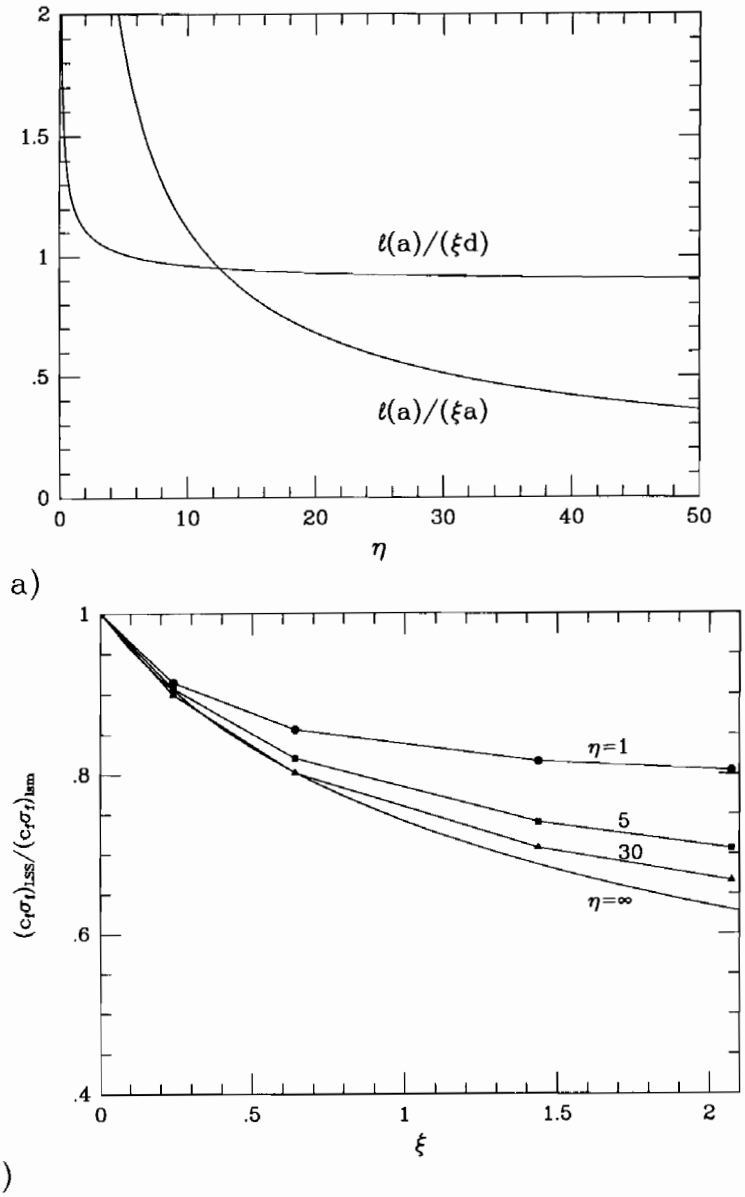

FIG. 7. (a) Normalized variation of the ratios of the height of the sliding zone at the tip of the through-crack, $l(a)$, to the crack half-length, a, and the length quantity, d, defined in (10), as predicted by the line–spring model. (b) Ratio of the bridging stresses just ahead of the through-crack tip from the two models cross-plotted against ξ for several values of η.

the 0° plies, as illustrated in Fig. 5(b). The plies are equally spaced with ply thickness $2t$, and the applied stress carried by the composite is σ. The pattern is doubly periodic with the spacing between cracks taken as $2L$. The sequence of events leading to an idealized pattern such as that envisioned in Fig. 5(b) is as follows. For the properties of a typical brittle-matrix cross-ply composite, the first cracks to form as the applied

stress is increased are those in the 90° plies which spread from flaws and tunnel in the direction perpendicular to the plane of Fig. 5(b). They extend all the way across the 90° plies. At higher applied stresses, these cracks serve as flaws from which plane strain matrix cracks spread across the 0° plies. The fibers in the 0° plies of a well designed composite must survive this process if the composite is to display any appreciable "ductility". The process just described has been analysed in some detail by XIA and HUTCHINSON (1994), who used a line–spring model to represent fiber bridging in the 0° plies. Their emphasis was on the applied stress associated with matrix cracking and the stress concentration in the most highly stressed fibers located at the ply interfaces. The doubly periodic cracking pattern shown in Fig. 5(b) is one of two patterns considered by Xia and Hutchinson to model crack interaction effects. The issue to be addressed here is whether the stresses predicted by the line–spring model for the most highly stressed fibers are unduly high, with clear implications for survivability of cross-plies with fully developed matrix cracks.

The fibers at the interfaces between the 90° and 0° plies will experience the highest stress. Again, define the stress concentration factor, λ, for these most highly stressed fibers by (15). The parametric dependence of this stress concentration factor has the general form

$$\lambda = \lambda\left(\frac{E_f}{E_m}, c_f, \eta, \frac{t}{L}\right), \tag{22}$$

where t/L is the crack density and η is now defined using t rather than a as

$$\eta = \frac{3\pi c_f^2 E_f E^2}{c_m^2 E_m^2 A\bar{E}} \frac{t\tau}{R_f\sigma}. \tag{23}$$

The dependence of λ on ν_f and ν_m is left implicit; $\nu_f = \nu_m = 0.2$ is used in the calculations.

In the case that the fibers and the matrix have identical elastic properties, the cross-ply is homogeneous and isotropic prior to any cracking. Solutions to the line–spring model version of the problem can be obtained by the integral equation techniques used by XIA and HUTCHINSON (1994). The results of the line–spring model for the SCF for the case $t/L = 0$ are shown in Fig. 8. Because all the load is carried by the bridging fibers in the 0° plies, λ is never less than 2. The stress concentration factors for the same problem obtained from the LSS model are also plotted in Fig. 8 for three values of c_f. The conclusion is that the line–spring model again overestimates the SCF in the range of practical values, sometimes significantly so.

Consider next the effect of the crack density, t/L, on the stress concentrations in the bridging fibers. An important consequence of multiple matrix cracking and sliding is the alleviation and ultimate elimination of the stress concentration in the fibers in the 0° plies. Elimination arises when the fibers are fully sliding (i.e. $l = L$ across the entire ply), as shown by elementary considerations of fiber equilibrium and stretching for the geometry in Fig. 5(b). An accurate estimate of the critical density of matrix cracks at which λ drops to 2 is obtained by setting $l = L$ and $p = 2\sigma$ in (3) giving

$$\left(\frac{t}{L}\right)_{crit} = \frac{c_f E t\tau}{c_m E_m R_f \sigma} = \frac{c_m E_m A\bar{E}}{3\pi c_f E_f E}\eta. \tag{24}$$

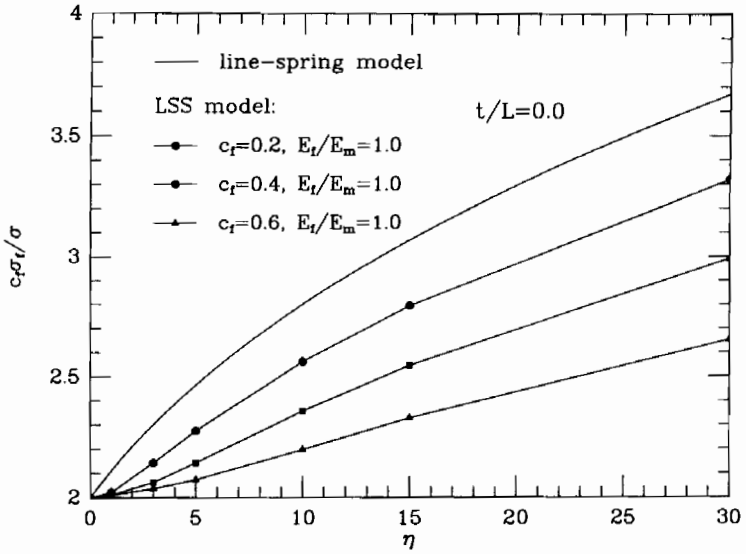

FIG. 8. Stress concentration factor for the bridging stress at the interface between the 0° and 90° plies of a cross-ply composite as predicted by the two models for the case $t/L = 0$. The line–spring prediction depends only on η defined in (23); the LSS prediction depends on η and on constituent parameters such as c_f and E_f/E_m.

Stated differently, as the applied stress σ increases, the matrix crack density increases until the fibers become fully sliding. In this state, the stress in each fiber where it bridges a matrix crack is given by $\sigma_f = 2\sigma/c_f$.

Numerical calculations based on the LSS model have been performed for a representative case of $E_f/E_m = 1$ and $c_f = 0.4$. Results for $\lambda = c_f\sigma_f/\sigma$ are plotted as a function of the crack density t/L for different values of η in Fig. 9. The numerical results are connected by dashed lines to the intercepts corresponding to first attainment of $\lambda = 2$ given by the formula (24). The accuracy of the simple formula is evident. Indeed, the numerical solutions revealed that the sliding zone approached the condition $l = L$ fairly uniformly across the 0° plies, as assumed in the derivation of (24).

In summary, as the applied stress on the cross-ply is increased, leading first to tunnel cracking in the 90° plies and then matrix cracking in the 0° plies, the stresses in the fibers at the ply interfaces will be the greatest. However, as the applied stress and the matrix crack density increase, the stress concentration *factor* for the fibers at the ply interfaces drops until matrix cracking is saturated with full sliding. In this state, the fibers uniformly share the load and the stress in the fibers at the matrix crack line becomes $\sigma_f = 2\sigma/c_f$.

6. The Experimental Situation

The ultimate tensile strengths (S_u) of many unidirectional and cross-ply CMCs have been reported to conform with predictions based on global load sharing (GLS) (Curtin, 1991). The GLS model considers that the load is distributed uniformly

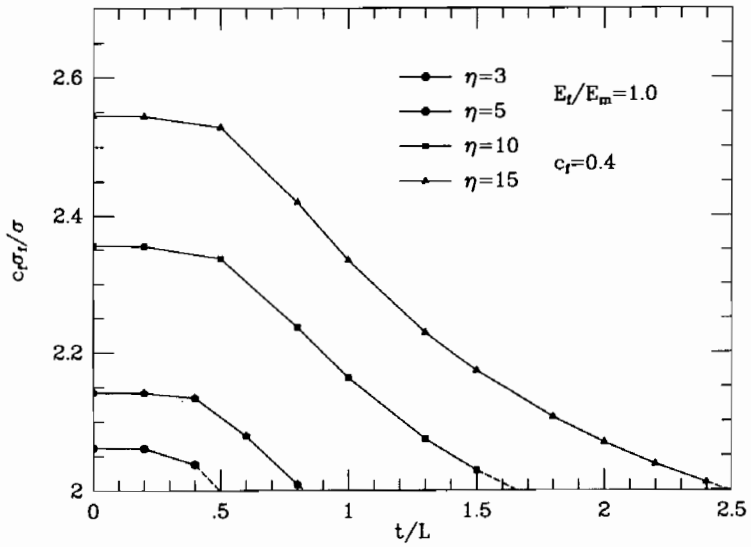

FIG. 9. Stress concentration factor for the bridging stress at the interface between the 0° plies and the 90° plies in a cross-ply composite as a function of crack density, t/L, as predicted by the LSS model. The intercept with the horizontal axis is given by (24).

among all intact fibers. The CMC materials that give good agreement with the GLS model include various SiC/C composites (HEREDIA *et al.*, 1992), SiC/CAS (PREWO, 1986) and SiC/CAS (BEYERLE *et al.*, 1992). Each of these materials has the common characteristic that the interface sliding stress τ is relatively small ($2 < \tau < 40$ MPa). The situation has been comprehensively summarized by CURTIN (1993). The implication of this agreement for the present discussion is that the stress concentration in the fibers is minimal at the failure loads, despite the presence of manufacturing flaws and matrix cracks. Otherwise, the stress concentration would lead to premature fiber failure and ultimate tensile strength values appreciably below the GLS predictions.

To explore the situation further, the preceding LSS model is used to evaluate the fiber stress concentration for various of the experimental conditions wherein GLS predictions have been found to apply. The most stringent test of the LSS model arises for cross-ply laminates. For this case, the unbridged crack dimension is the largest (the ply dimension $2t$), resulting in correspondingly large values of η (23). Experimental information for several CMCs is summarized in Table 1. These experimental characteristics can be most readily compared with the LSS model by using (24), with $\sigma = S_u$, to predict the crack spacing at which the stress concentration in the fibers is eliminated.

TABLE 1. *Properties of cross-ply CMCs*

Material	E_m (GPA)	τ (MPa)	S_u (MPa)	η	$c_f\sigma_f/\sigma$	$(t/L)_{crit}$
SiC/C	20	10	340	90	≈ 2	1.03
SiC/CAS	100	15	220	10	2	0.81
SiC/LAS	100	3	300	1	2	0.08

$E_f = 200$ GPa; $R_f = 7$ μm; $c_f = 0.4$, $c_m = 0.6$.

For all three composites, $(t/L)_{crit}$ is about unity or less (Table 1). Crack spacings in CMCs almost invariably satisfy $t/L > 1$ prior to composite rupture (BEYERLE *et al.*, 1992; GUILLAUMAT, 1993). The applicability of the GLS criterion for the ultimate tensile strength is thus consistent with the predictions of the LSS model. One other factor is relevant for the SiC/C composite, which gives the largest $(t/L)_{crit}$ (Table 1). Processing flaws tend to induce inter-ply shear cracks (TURNER *et al.*, 1993) which suppress matrix cracks in the 0° plies, while also eliminating stress concentrations in the fibers.

The comparison with experiments has emphasized the importance of large scale sliding in governing the stresses in fibers within cross-ply composites, resulting in the applicability of global load sharing concepts for predicting the ultimate tensile stress. Related arguments would apply regarding the role of manufacturing flaws within the plies. Such flaws result in unbridged cracks, which would be expected to introduce stress concentrations into the fibers. The line–spring model and the LSS results taken together show that, where these stress concentrations exist, they can be relatively small provided that η is less than about 3 (cf. Fig. 6), especially when E_f/E_m is large. The clear implication from (16) is that the material becomes more tolerant to manufacturing flaws when the interface sliding resistance is low.

ACKNOWLEDGEMENTS

This work was partially supported by the DARPA University Research Initiative ONR Prime Contact N00014-91-J-1808, by the NSF through grant DMR-89-20490, and by the Division of Applied Sciences, Harvard University.

REFERENCES

AVESTON, J., COOPER, G. A. and KELLY, A. (1971) Single and multiple fracture. *The Properties of Fiber Composites*, pp. 15–26. Proc. National Physical Laboratory, Guildford, IPC Science and Technology, U.K.

BAO, G. and SUO, Z. (1992) Remarks on crack-bridging concepts. *Appl. Mech. Rev.* **24,** 355–366.

BEYERLE, D. S., SPEARING, S. M. and EVANS, A. G. (1992) Damage mechanisms and the mechanical properties of a laminated 0/90 ceramic/matrix composite. *J. Am. Ceram. Soc.* **75,** 3321–3330.

BUDIANSKY, B. and CUI, Y. L. (1994) On the tensile strength of a fiber-reinforced ceramic composite containing a crack-like flaw. *J. Mech. Phys. Solids* **42,** 1–19.

BUDIANSKY, B., HUTCHINSON, J. W. and EVANS, A. G. (1986) Matrix fracture in fiber-reinforced ceramics. *J. Mech. Phys. Solids* **34,** 167–189.

CURTIN, W. A. (1993) The tough to brittle transition in brittle matrix composites. *J. Mech. Phys. Solids* **41,** 217–221.

CURTIN, W. A. (1991) The ultimate strength of ceramic matrix composites. *J. Am. Ceram. Soc.* **74,** 2037–2041.

GUILLAUMAT, L. (1993) Ph.D. Thesis, Laboratoire des Composites Thermostructuraux, Domaine Universitaire, Bordeaux, France.

HE, M. Y., WU, B. X., EVANS, A. G. and HUTCHINSON, J. W. (1993) Inelastic strains due to matrix cracking in unidirectional fiber-reinforced composites. *Mech. Mater.*, in press.

HEREDIA, F. E., SPEARING, S. M., EVANS, A. G., MOSHER, P. and CURTIN, W. A. (1992) The

mechanical properties of continuous fiber reinforced ceramic composites. *J. Am. Ceram. Soc.* **75,** 3321–3327.

HILL, R. (1965) Theory of mechanical properties of fiber-strengthened materials—III. Self-consistent model. *J. Mech. Phys. Solids* **13,** 189–198.

MARSHALL, D. B. and COX, B. N. (1987) Tensile fracture of brittle matrix composites: influence of fiber strength. *Acta Met.* **35,** 2607–2619.

MARSHALL, D. B. and COX, B. N. (1988) A *J*-integral method for calculating steady-state matrix cracking stress in composites. *Mech. Mater.* **7,** 127–133.

MARSHALL, D. B., COX, B. N. and EVANS, A. G. (1985) The mechanics of matrix cracking in brittle-matrix fiber composites. *Acta Met.* **33,** 2013–2021.

MCCARTNEY, L. N. (1987) Mechanics of matrix cracking in brittle-matrix fibre-reinforced composites. *Proc. R. Soc. Lond.* **A409,** 329–350.

MEDA, G. and STEIF, P. S. (1993) A detailed analysis of cracks bridged by fibers—Part II. Cracks of intermediate size. *J. Mech. Phys. Solids*, in press.

PREWO, K. (1986) Tension and flexural strength of silicon carbide fiber reinforced glass ceramics. *J. Mater. Sci.* **21,** 3590–3597.

TURNER, K. S., SPECK, J. S. and EVANS, A. G. (1993) The tensile and shear properties of carbon matrix composites, submitted to *J. Am. Ceram. Soc.*

XIA, Z. C. and HUTCHINSON, J. W. (1994) Matrix cracking of cross-ply ceramic composites. *Acta Met. Mater.*, in press.